

Simultaneous P-P and P-S waveform inversion algorithm using Pre-Stack time imaging method

Hassan Khaniani, John C. Bancroft and Eric von Lunen

ABSTRACT

The conventional approach of elastic Full Waveform Inversion (FWI) requires a forward modeling and a depth migration. The forward modeling engine, which is usually based on a finite difference solution of the elastic wave equation, computes the data residual that compares the data derived from the current model with the real data from the true model. Migration is an adjoint operator of the forward modeling, which is usually based on Reverse Time Migration (RTM) on the data residual, and finds the gradient function from the current model toward the true model.

Numerically, this scheme suffers from huge computational costs associated with the time stepping of forward modeling and the migration. Assuming multiple free data and smooth lateral variation of subsurface properties, this work serves as an introduction to elastic waveform inversion using Pre-Stack Time Migration (PSTM) and the corresponding forward modeling.

INTRODUCTION

Seismic FWI was introduced by Tarantola (1984) to estimate high resolution subsurface properties from waveform information contained in seismic data. FWI is a least-squares approach to minimize the differences between synthetic and observed data during the updating of the model parameters.

Several authors have undertaken full waveform inversion in the time domain based on finite difference solution to elastic waveform inversion. To study the long history of FWI the reader is referred to Virieux and Operto (2009) and Sears et al (2007).

This work is based on the conclusion of Tarantola (1984) that showed that classical Kirchhoff migration and corresponding forward modeling can be used in the FWI procedure. Our effort is to reduce the computational costs associated with gradient calculation and data prediction. In other work we have described the use of forward Pre-Stack time Kirchhoff operator for the prediction of P-P data from the reflectivity function (i.e. Schneider, 1978, Bleistein et. al., 2001) and the corresponding PSTM migration for the inversion process in FWI algorithm (Khaniani et al., 2012).

The mathematical expressions of the linearized inverse scattering problem in this paper are mainly cited from Beylkin and Burridge (1990). The inversion expression used in this work is mathematically expressed on a least-squares minimization proposed by Tarantola (1984, 1996 and 1987).

Using the elastic inversion schemes that usually require the inversion of the model parameters in depth, we have developed an algorithm that predicts the mode converted P-S wave using the velocity in time. The algorithm is based on the scatter point response in

P-wave reflection intercept time. This facilitates the updating process using the parameters of traveltimes and amplitudes of scatter points.

The methodology is fast compared to corresponding depth migration techniques in forward and inverse iterations however, since we are doing time migration, we are limited to models with moderate complexity. In this work, we assume the data are multiple free because of limitation in the forward and adjoint operator to handle the multiple data.

FORWARD PROBLEM FOR ACOUSTIC REFLECTED WAVE

In an acoustic medium, the pressure field $U(s, x, t)$ satisfies the equation

$$\left(\frac{1}{C^2(x)} \frac{\partial^2}{\partial t^2} - \nabla^2 \right) U(x, t) = S(x, t), \quad (1)$$

where $C(x)$ is the velocity of the acoustic wave in the subsurface coordinate x , and $S(x, t)$ is the source component injected into the medium at time t .

Using a casual Green's function $G(x, t, x', t')$ satisfying equation (1)

$$\left(\frac{1}{C^2(x)} \frac{\partial^2}{\partial t^2} - \nabla^2 \right) G(x, t, x', t') = \delta(x - x') \delta(t - t'), \quad (2)$$

the problem can be simplified to reflected P-P wave by defining $G(x, t, x', t')$ to be

$$G(x, t, x', t') = K^{PP} \delta(t - t' - \phi(s, r)), \quad (3)$$

where s and r are source and receiver position, and $\phi(s, r)$ is the total traveltimes from s to the r which is reflected from x

$$\phi(s, r) = \phi(s, x) + \phi(x, r), \quad (4)$$

where $\phi(s, x)$ is traveltimes from s to the scatter point located at x and $\phi(x, r)$ is the traveltimes from x to receiver r . The parameter K^{PP} is an amplitude term and is approximated by the amplitude loss of the P-wave propagated from s to x (i.e., $A^P(s, x)$) and from x to r (i.e., $A^P(x, r)$)

$$K^{PP} = A^P(s, x) A^P(x, r) = \frac{1}{\|s - x\|} \frac{1}{\|x - r\|}. \quad (5)$$

By adding the background medium $C(x)$ with the small perturbation $\Delta C(x)$ (i.e., $|\Delta C| \ll C$), we get the Taylor series expansion of perturbed medium given by

$$\frac{1}{(C(x) + \Delta C(x))^2} = \frac{1}{C^2(x)} - \frac{2\Delta C(x)}{C^3(x)} + o(\Delta C(x)). \quad (6)$$

The term o is a higher order approximation of the Taylor series expansion. The difference between the wavefield corresponding to the true medium $U_{C+\Delta C}^{PP}$ and the one corresponding wavefield in the homogeneous reference medium U_C^{PP} is the scattered field $U_{\Delta C}^{PP}$ due to a perturbation ΔC (Tarantola (1984, 1986), Beylkin and Burridge (1990))

$$\Delta U_{\Delta C}^{PP} = U_{C+\Delta C}^{PP} - U_C^{PP} = \partial_t^2 \int dx' K^{PP} \frac{2\Delta C(x')}{C^3(x')} \delta(t - \phi(s, x') - \phi(x', r)) S(t). \quad (7)$$

The term $\Delta U_{\Delta C}^{PP}$ is the scattered field and does not contain the unperturbed field due to the background medium.

INVERSE PROBLEM FOR ACOUSTIC REFLECTED WAVE

Beylkin and Burridge (1990) derived the direct inversion for $\Delta C(x)$ considering the forward operator f of the integral function in (7) as a generalized Radon transform (see also Bleistein et al (2001). Tarantola (1986) used an alternative approach that uses the concept of a generalized nonlinear least-squares inverse problem to minimize an objective function S defined by

$$S = \|\Delta U_{\Delta C}^{PP}\|^2 = \|U_{obs}^{PP} - U_C^{PP}\|^2, \quad (8)$$

where, U_{obs}^{PP} is approximation of $U_{C+\Delta C}^{PP}$. In order to simplify the problem, the density is assumed to be constant, even though it is variable over ΔC . Tarantola (1986) considered the integral function in (7) as a forward operator f on $\Delta C(x)$, (i.e., $\Delta U_{\Delta C}^{PP} = f(\Delta C)$) and used a linear operator F as the derivative of f at the point C (i.e., $F = \frac{\partial f}{\partial C}$)

$$f(C + \Delta C) = f(C) + F\Delta C + o(\|\Delta C\|^2), \quad (9)$$

which has a solution of

$$C_{k+1} = C_k - \alpha \gamma_k, \quad (10)$$

with γ_k to be the gradient function to minimize (8) and defined by

$$-\gamma_k = -\frac{\partial S}{\partial C} = c_m F^* c_p^{-1} [\Delta U_{\Delta C}^{PP}], \quad (11)$$

where c_m and c_p are the general covariance operator corresponding to a priori model and data sets measurements (Tarantola, 1986). In each iteration of the algorithm the model is updated using the two following steps:

1. Perform forward modeling for computation of scattered data (i.e., $\Delta U_{\Delta C}^{PP} = f(\Delta C)$)

2. Perform the data residual backward in time and correlate the upgoing and downgoing wavefield at each scatter point. This resembles the migration method based on the imaging principle of Claerbout (1971) over the data residual (i.e., $F^*(\Delta U_{\Delta C}^{PP})$).

Equations (7) and (10) are within the medium that the velocity model $C(x)$ needs to be inverted having an initial model $C(x)$ and the scattered field $\Delta U_{\Delta C}^{PP}$. Using a least squares fitting approach, the update procedure requires a forward modeling to have a velocity model in depth (i.e., $C(x)$) and a corresponding depth migration that requires traveltime $\phi(s, r)$. $\phi(s, r)$ can also be obtained by ray tracing Tarantola (1986) or PSPI (Margrave et al., 2011).

The implementation of time imaging forward modeling and corresponding migration is discussed in another paper (Khaniani et al., 2012). In the geological models with smooth lateral variations in velocity, approximation of $\phi(s, r)$ can be obtained using the Double Square Root (DSR) equation (Yilmaz, 2001)

$$\phi^{PP}(s, r) = \sqrt{\frac{\tau^2}{4} + \frac{(X+h)^2}{v_{rms}^P}} + \sqrt{\frac{\tau^2}{4} + \frac{(X-h)^2}{v_{rms}^P}}, \quad (12)$$

where τ is the zero offset two-way travel time, h is the half source/receiver offset, X is the distance from the source/receiver midpoint to the lateral coordination of the scatter point and $v_{rms}^P(\tau, x)$ is the migration velocity that is defined in time instead of depth. In this approach, the forward modeling and migration are designed based on equation (12) so, the velocity $C(\tau, x)$ is updated on time by $\Delta C(\tau, x)$.

FORWARD PROBLEM FOR ELASTIC REFLECTED WAVE

Wave propagation in an inhomogeneous anisotropic elastic solid in the absence of source is

$$\rho(x)\partial_t^2 U_l - (c_{lmpq}(x)U(x, t)_{p,q})_{,m} = 0, \quad (13)$$

where $U_l(x, t)$ is the l -component of the displacement vector, $\rho(x)$ is density and $c_{lmpq}(x)$ are the elastic constant of the subsurface medium and x is subsurface coordinate. For a 2D, continuous, elastic wave equation in a homogeneous, isotropic medium the elastic constant are simplified as

$$c_{lmpq} = \lambda \delta_{lm} \delta_{pq} + \mu (\delta_{lp} \delta_{mq} + \delta_{lq} \delta_{mp}), \quad (14)$$

where λ and μ are lame's constant and here δ_{lp} are Kronecker delta function. Then the equation (13) can be expressed by a pair of equations (Manning, 2007),

$$(\lambda + 2\mu) \frac{\partial^2 U_z}{\partial z^2} + (\lambda + \mu) \frac{\partial^2 U_x}{\partial x \partial z} + \mu \frac{\partial^2 U_z}{\partial x^2} = \rho \frac{\partial^2 U_z}{\partial t^2}, \quad (15)$$

and

$$(\lambda + 2\mu) \frac{\partial^2 U_x}{\partial x^2} + (\lambda + \mu) \frac{\partial^2 U_z}{\partial x \partial z} + \mu \frac{\partial^2 U_x}{\partial z^2} = \rho \frac{\partial^2 U_x}{\partial t^2}, \quad (16)$$

where U_x and U_z are the horizontal and vertical displacements of the particle motion respectively. Figure (1) shows an example wavefield snap created by an explosion source injected in the medium. The direct P- wave reflected and transmitted P-P and P-S waves are illustrated.

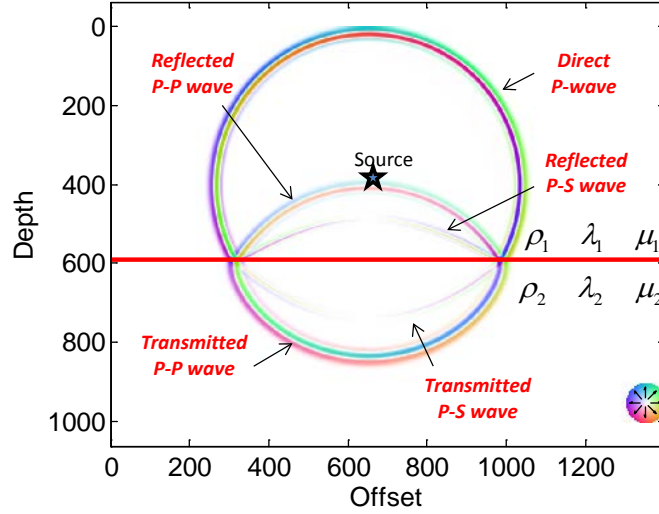


FIG. 1: Elastic wave propagation. A snap produced by a P- wave producing reflected and transmitted P-P and P-S.

Let $G_{jl} = G_{jl}(s, x, t)$ be the incident field which satisfies the following equation:

$$\begin{aligned} \rho \partial_t^2 G_{jl} - (c_{lmpq} G_{jp,q})_{,m} &= \delta_{jl} \delta(t) \delta(x-s), \\ G_{jl} \Big|_{t < 0} &= 0. \end{aligned} \quad (17)$$

Here, G_{jl} is the displacement in the l -direction at point x due to a point source in j^{th} direction at point s . Beylkin (1990) derived high frequency approximation of the integral representation of the single scattered field using

$$\begin{aligned} \rho_{true} &= \rho + \Delta\rho, \\ \lambda_{true} &= \lambda + \Delta\lambda, \\ \mu_{true} &= \mu + \Delta\mu. \end{aligned} \quad (18)$$

to get

$$\Delta U_{jk}(s, r, t) = \Delta U_{jk}^{PP}(s, r, t) + \Delta U_{jk}^{PS}(s, r, t) + \Delta U_{jk}^{SP}(s, r, t) + \Delta U_{jk}^{SS}(s, r, t), \quad (19)$$

where ΔU_{jk}^{PP} is the scattered P-P data (same as equation (7) for constant ρ)

$$\Delta U_{jk}^{PP} = -\partial_t^2 \int \rho^0 \left[\frac{\Delta\lambda}{\lambda + 2\mu} + \frac{\Delta\rho}{\rho} \cos \theta^{PP} + \frac{2\Delta\mu}{\lambda + 2\mu} \cos^2 \theta^{PP} \right] A_j^P A_k^P \delta(t - \phi^P - \phi^P) dx. \quad (20)$$

The scattered P-S wave ΔU_{jk}^{PS} is

$$\Delta U_{jk}^{PS} = -\partial_t^2 \int_D \rho^0 \left[\frac{\Delta\rho}{\rho} \sin \theta^{PS} + \frac{\Delta\mu}{\mu} \frac{c_S}{c_P} \sin 2\theta^{PS} \right] A_j^P A_k^S \beta_l^{PS} \delta(t - \phi^P - \phi^S) dx, \quad (21)$$

and ΔU_{jk}^{SP} is scattered energy if the source is shear wave

$$\Delta U_{jk}^{SP} = -\partial_t^2 \int_D \rho^0 \left[\frac{\Delta\rho}{\rho} \sin \theta^{SP} + \frac{\Delta\mu}{\mu} \frac{c_S}{c_P} \sin 2\theta^{SP} \right] A_{jp}^S \beta_p^{SP} A_k^P \delta(t - \phi^S - \phi^P) dx, \quad (22)$$

and finally the ΔU_{jk}^{SS} is combination of reflected S-wave and mode converted S- wave

$$\begin{aligned} \Delta U_{jk}^{SS} = & -\partial_t^2 \int_D \rho^0 \left[\frac{\Delta\rho}{\rho} \cos \theta^{SS} + \frac{\Delta\mu}{\mu} \cos 2\theta^{SS} \right] A_{jp}^S \beta_p^{SS} A_{kl}^S \delta(t - \phi^S - \phi^S) dx \\ & - \partial_t^2 \int_D \rho^0 \left[\frac{\Delta\rho}{\rho} + \frac{\Delta\mu}{\mu} \cos \theta^{SS} \right] A_{jp}^S \gamma_p^{SS} A_{kl}^S \gamma_l^{SS} \delta(t - \phi^S - \phi^S) dx. \end{aligned} \quad (23)$$

Equations (20) to (23) are the perturbed waves in the shot records due to the perturbed elastic properties of the medium. The terms inside the bracket describes their radiation patterns. In this work we perform the inversion scheme on only P-P and P-S waves and ignore the effects of S-P and S-S waves because of the source mechanisms and attenuation pattern make their amplitude small compared to P-P and P-S waves.

INVERSE PROBLEM FOR ELASTIC REFLECTED WAVE

As proposed by Tarantola (1996) the least squares criterion for the elastic inversion

$$S = \frac{1}{2} \left(\|U - U_{true}\|^2 \right), \quad (24)$$

Here, U represents the data predicted by the model parameters m (i.e., ρC^P , ρC^S and ρ) similar to the acoustic procedure, Tarantola (1994) suggested the method of steepest descent algorithm for the inversion of the model parameters.

$$m(x)_{n+1} = m(x)_n - \alpha \gamma_n(x), \quad (25)$$

which minimizes the equation (24). His suggested algorithm includes the following two main steps:

1. Forward modeling for calculation of data residuals $\Delta U(r, t; s)$ by

$$\Delta U(r, t; s)_n = \frac{U^i(r, t; s)_n - U^i(r, t; s)_{obs}}{\sigma^2(r, t; s)}, \quad (26)$$

which requires forward modeling of different waves using equation (20) to (23). This step is used for calculation of α .

2. Depth migration of data residuals for gradient calculation $\gamma_n(x)$. This step is done by applying an “imaging principle” with forward propagation of the source $U^{ii}(x, t; s)$ and back propagation in time of $\Delta\psi(x, t; s)$

$$\gamma_n(x) = \sum_s \int_0^T dt U^{ii}(x, t; s)_n \times \Delta\psi^{jj}(x, t; s)_n, \quad (27)$$

where, $\Delta\psi^{jj}(x, t; x_s)_n$ is back propagated in time using a Green’s function $G^{jj}(x, 0; x_s, t)$ which satisfies equation (17)

$$\Delta\psi(x, t; s)_n = \sum G^{jj}(x, 0; r, t) * \Delta U^j(r, t; s)_n. \quad (28)$$

TIME IMAGING CONSIDERATIONS FOR INVERSE PROBLEM FOR ELASTIC REFLECTED WAVE

In equation(28), the Green function $G^{jj}(x, 0; r, t)$ is useful for analytical developments, but it never has to be used explicitly in numerical computation (Tarantola, 1996). Using a similar form of equation (7) in the form of equations (20) - (23), the method of the waveform inversion requires applying a forward operator to create the data (circle summation) and a migration based on hyperbola summation of scattered data.

This is based on the generalized solution of Tarantola (1984), but contains forward modeling and migration of scatter point responses using the time migration algorithm. In this approximation the associated traveltimes are calculated from Root Mean Square (RMS) velocity. The amplitude function is obtained using an estimation of reflectivity function obtained from the Zoeppritz solvers (Aki and Richards, 1980). Assuming lower amplitude of S-P and S-S data from the injected source in z-component, in this work, the forward operator is designed only for reflection data of P-P and P-S data. In the forward modeling, the traveltime for P-P data is approximated by

$$t^{pp} \approx \phi^P(s, x) + \phi^P(x, r) = \frac{r(s, x)}{v_{RMS}^P} + \frac{r(x, r)}{v_{RMS}^P}, \quad (29)$$

and the traveltime for the P-S data is obtained by

$$t^{ps} \approx \phi^P(s, x) + \phi^S(x, r) = \frac{r(s, x)}{v_{RMS}^P} + \frac{r(x, r)}{v_{RMS}^S}. \quad (30)$$

To study the different methodologies for converted wave data processing and migration the reader is referred to Mi and Margrave (2001). A common approach for the time migration of P-S data is to find the image based on Common Converted Point (CCP), this

ultimately maps the energy on P-S time. This procedure is useful during imaging if the shear velocity of the subsurface is unknown. We displayed the graphical representation of this approach on a synthetic model shown in Figure (2). Here, the C^P and C^S of the medium are plotted versus t^{PP} and t^{PS} respectively. Figure (2b) shows the migrated section of the data obtained from Figure (2a). This shows that the P-S data space is mapped to the model space in t^{PS} coordinate, inferring that after imaging both P-P and P-S waves, a P-P and P-S registration are required to identify the events for interpretation.

To perform the waveform inversion, we need to implement both traveltime and amplitude considerations during forward modeling and migration of both P-P and P-S waves. Therefore, for the migration operator as the adjoint of the forward operator, we design an algorithm that considers the common traveltime for the scatter point, $\phi^P(s, x)$. Then, at each scatter point, the algorithm sums the hyperbola corresponding to t^{PP} and t^{PS} for P-P and P-S data respectively. Hence, the migration operators for P-P and P-S data maps the data to the model space, τ , in the same time coordinate. This facilitates computation of the gradient function for P-P and P-S data.

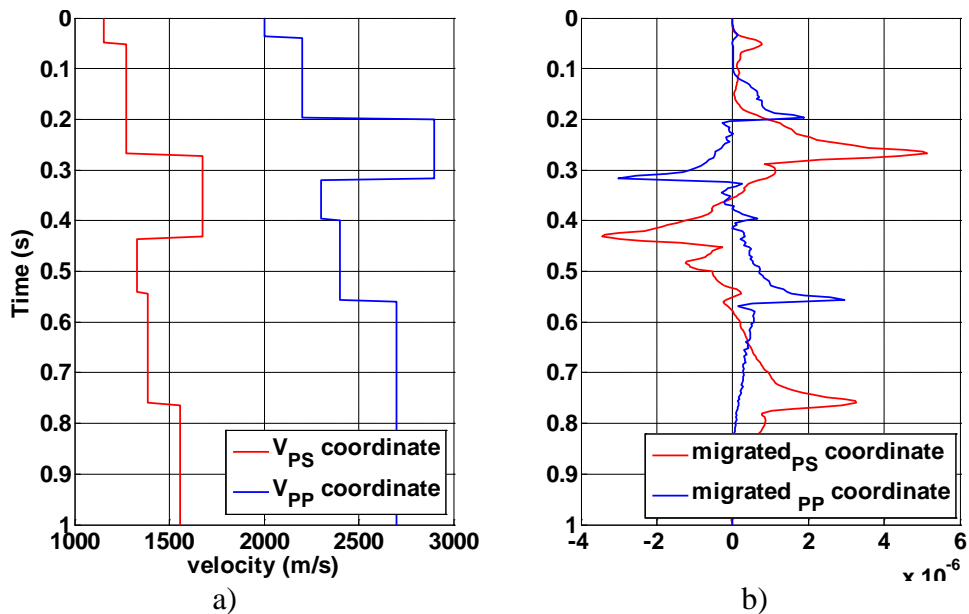


Fig. 2: Inconsistency between time of velocity model vs migrated CCP a) velocity profile of P and S in P-P and P-S time b) migration of P-P and P-S data in P-P and P-S time.

Figure(3) shows a single shot record on the vertical component of the elastic forward operator over a simple geological model with a single reflector. Figure (3a) is obtained by a finite difference solution of a pair of equations (15) and (16). Figure (3b) is obtained with the solution of the elastic Kirchhoff solution to the same model. The amplitude and traveltime of direct P-wave, S-waves and the reflected P-P and P-S waves obtained from the Kirchhoff is consistent with that obtained from the finite difference. For example, the shear wave has zero amplitude near the zero-offset positions as determined by the Zoeppritz solvers inside the algorithm.

The migration result of the modeled data as the adjoint of the forward operator for P-P and P-S waves are shown in figures (3c) and (3d) respectively. Both P-P and P-S data are mapped on the same P- time $\phi(s, x)$.

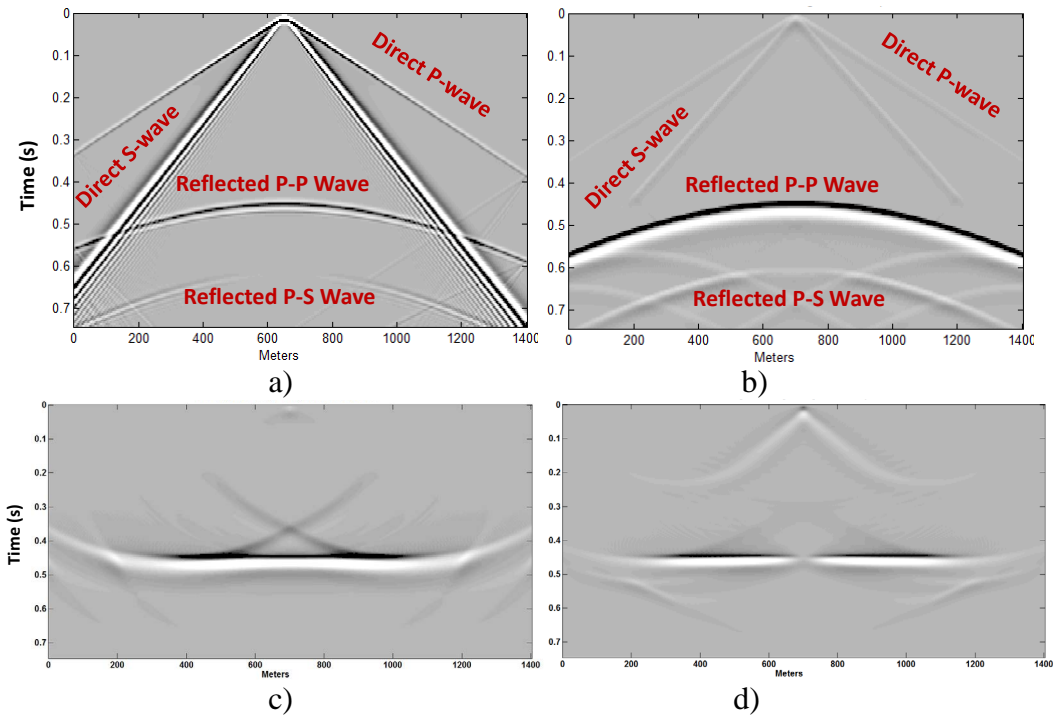


FIG. 3: Forward modeling vs migration of P-P and P-S data based on P-P time. a) a shot record simulated by finite difference solution of elastic wave equation b) a shot record simulated by Kirchhoff solution of elastic wave equation c) P-P data migrated in P- time $\phi(s, x)$ d) P-S data migrated in P- time $\phi(s, x)$.

In figure (4) the flowchart of the developed algorithm for elastic inversion is illustrated. The algorithm begins with an acoustic inversion using time migration procedure. We can set up the program to perform the inversion on P-P data to obtain the C^P and then perform the P-S inversion to calculate the C^S . The alternative approach is to do the inversion simultaneously so that at each step the model update for P-P data is used for updating the model in P-S algorithm.

Figure (5) shows a synthetic waveform inversion result from a synthetic model. Note that the geologic model $C^P(\tau, x)$ and $C^S(\tau, x)$, are defined in the same time, which is consistent with the time of the event found in the inverted model. In Figures (6a) and (6b), all of the variations in the RMS velocities V_{RMS}^P and V_{RMS}^S during all iterations are shown. This shows the stability of the updates obtained from Kirchhoff migration as the traveltimes change in equations (29) and (30).

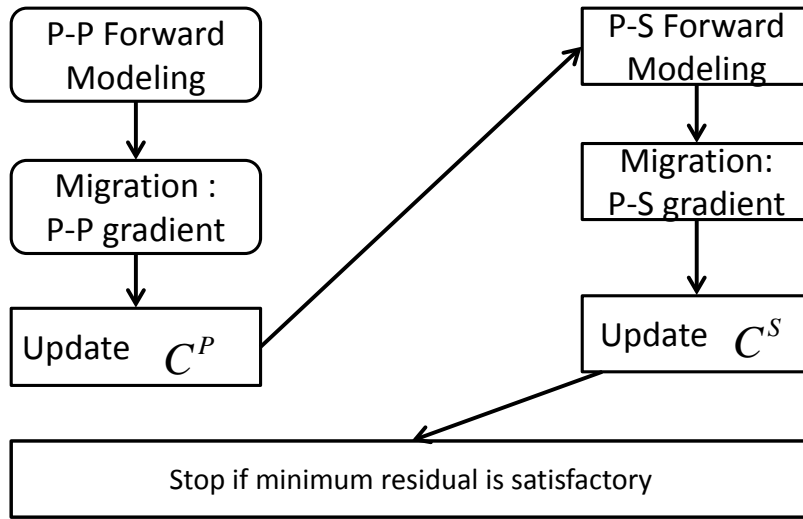


FIG. 4: simplified simultaneous inversion of P-P and P-S for P- and S-wave velocity

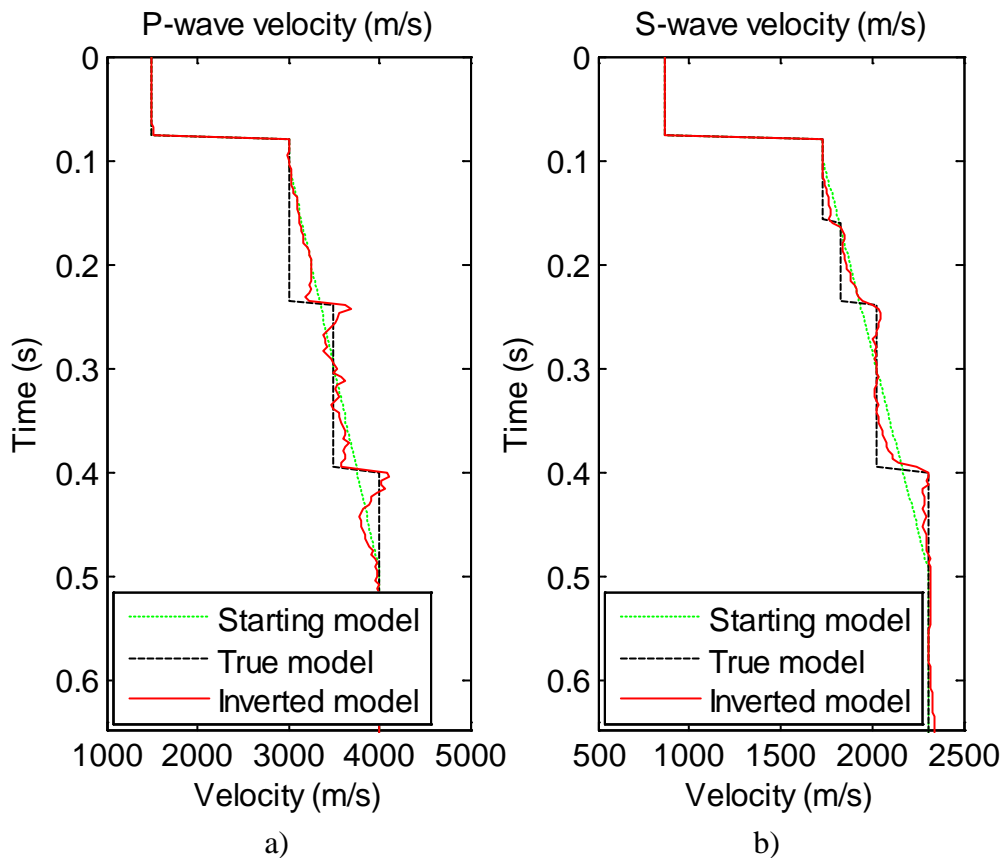


FIG.5: inversion result of P- and S-wave velocity. a) P-wave inversion b) S- wave velocity

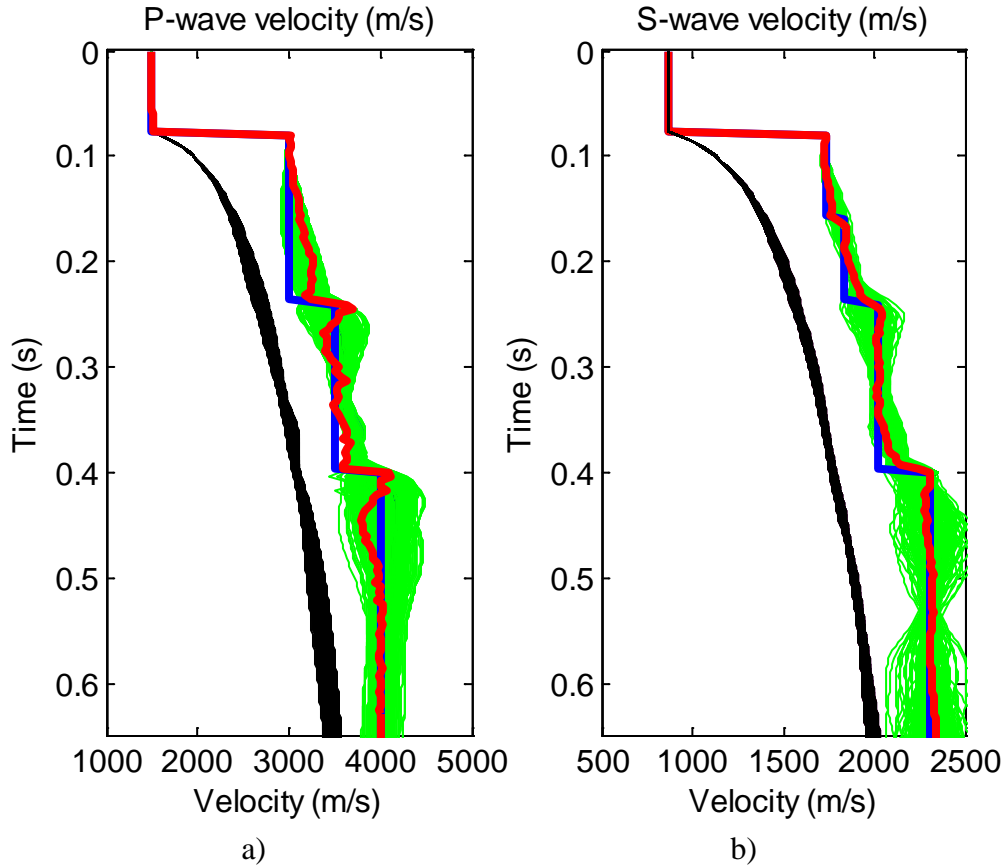


FIG.6: Stability of Time imaging during inversion a) comparison of the P- wave velocity inversion result (red line), with true velocity profile (blue line), the iteration variation of C^P (green) and V_{RMS}^P (black line) b) comparison of the S- wave velocity inversion result (red line), with true velocity profile (blue line), the iterations variation of C^S (green) and V_{RMS}^S (black line).

FORWARD MODELING AND MIGRATION OF FIELD DATA

Figure (7a) shows the migration result of a field vertical component (P-P dominant) of 51 shot records in NE-BC acquired by Nexen Inc. For a comparison, as shown in Figure (7b), the modeled shot records were migrated with the same migration algorithm used for field P-P data in Figure (7a). Figure (7c) shows the radial component (P-S dominant) data of the same shot records migrated using t^{PS} defined in equation (30). The velocity for migration is obtained by well log information shown in Figure (8a). Since the area has smooth lateral variation in velocity, we modeled the shot records using $C^P(\tau, x)$ and $C^S(\tau, x)$ from well log. The small difference in time of the migrated sections is due to the different static correction datum used during the processing.

Figure (8) compares the migration and the forward modeling of P-S data based on the Zoeppritz solver implemented in the program. It can be seen that the radiation pattern of the reflected P-S events (e.g. events A, B, C, D and E) in Figure (8b) are consistent with the events in the migrated field P-S data shown in Figure (8c). This is because of the radiation pattern of P-S data is angle dependant.

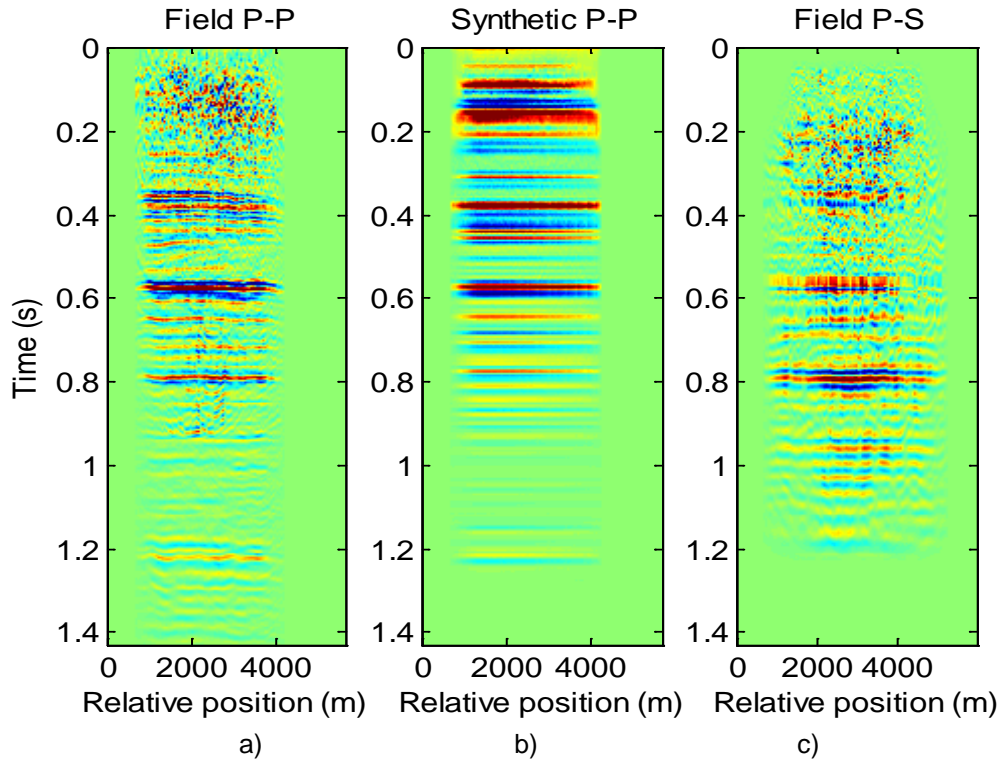


FIG. 7: comparison of Migration result in P- time $\phi(s, x)$. a) migrated field P-P data b) migrated synthetic P-P data c) migrated field P-S data

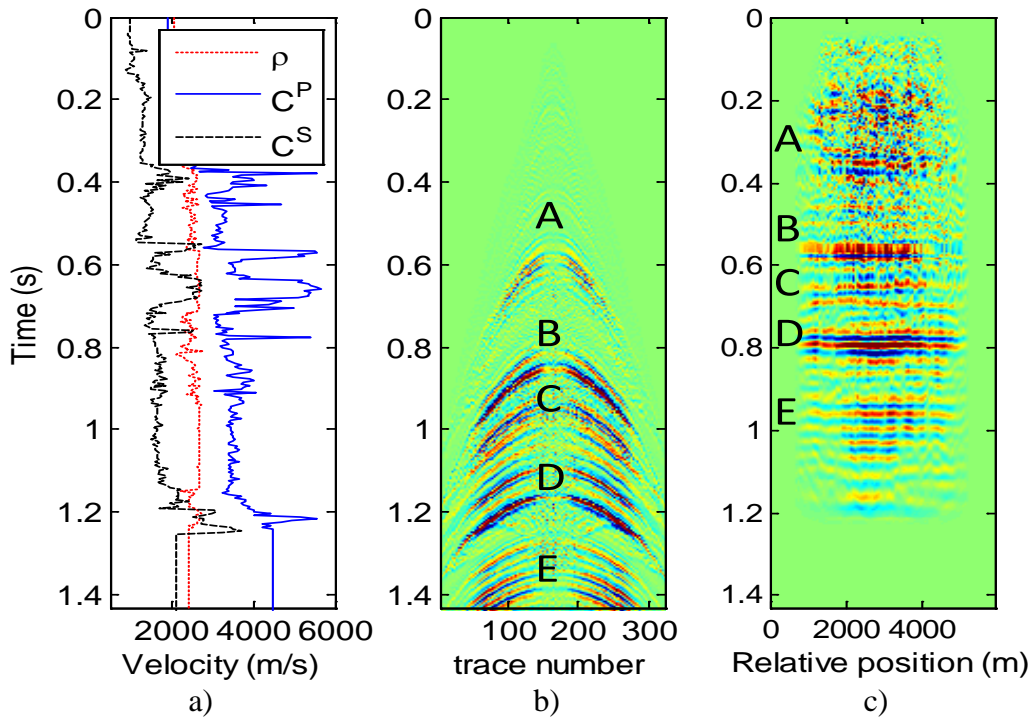


FIG. 8: Forward modeling result and the angle dependency of P-S waves. a) well log information b) modeled P-S Shot data c) migrated field P-S data on P- time $\phi(s, x)$.

We note that our waveform inversion is based on linearization of seismic reflection data as expressed by equations(19). In the field data we will have to eliminate the noise in order to minimize the objective function defined by equation (24). Noise in this case, are any signals that are not of interest and are not included in the forward modeling. Examples of noise are multiple data, surface waves, surface noise and dead traces. In Figure (9), we compare one sample shot record before and after processing. The key factor for processing is to preserve the original amplitude. This can be seen by comparing the strong reflector across the center of the raw shot (Figure 9a) and processed shot (Figure 9b).

The radial component data of a sample shot is currently under process. We aim to improve the Signal to Noise Ratio (SNR). Figure (9c) shows the raw radial component acquired near the record shown in Figure (9a). So far, the processed radial component is shown in Figure (9d) for the inversion of P-S data parameters. Additional processing will follow in the future.

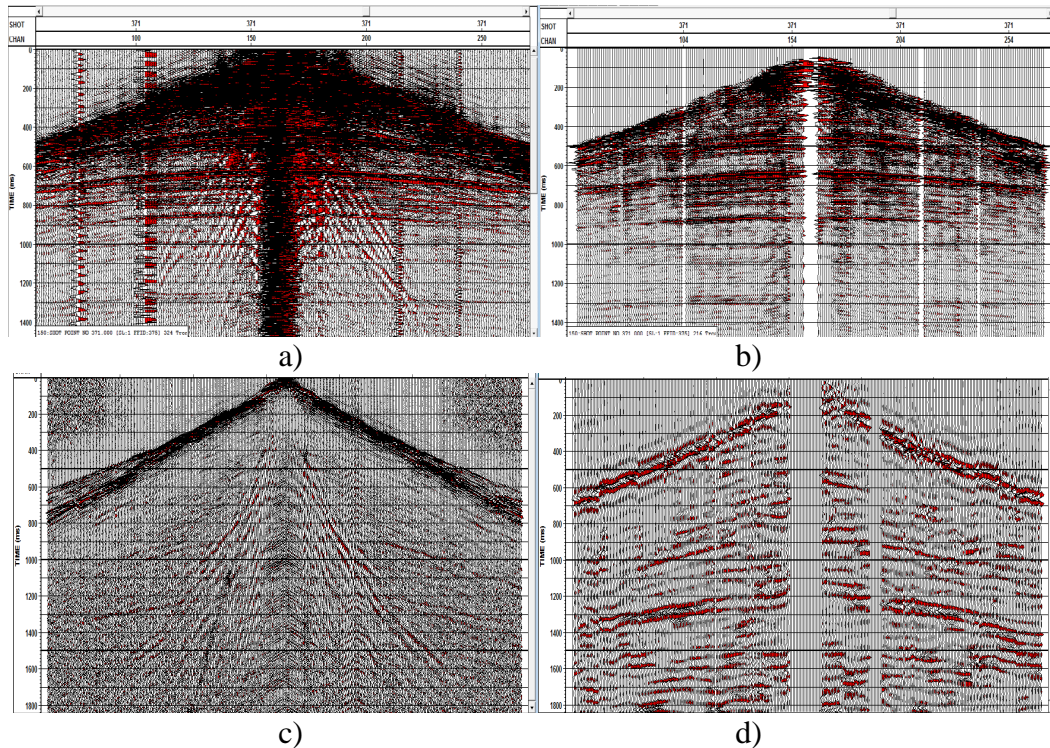


FIG. 9: Processing of reflection vertical and radial component a) Raw shot on vertical component b) processed vertical component c) Raw shot on radial component. (AGC applied for illustrations) d) processed radial component (AGC applied for illustrations).

The preliminary result of velocity inversion is shown in Figure (10). The initial velocity for inversion of $C^P(\tau, x)$ is obtained using a linear increment (green dotted line) of the well log (solid blue curve) contained in Figure (10). We inverted for the data after 0.5s because our migration algorithm is limited to migration of deeper reflectors.

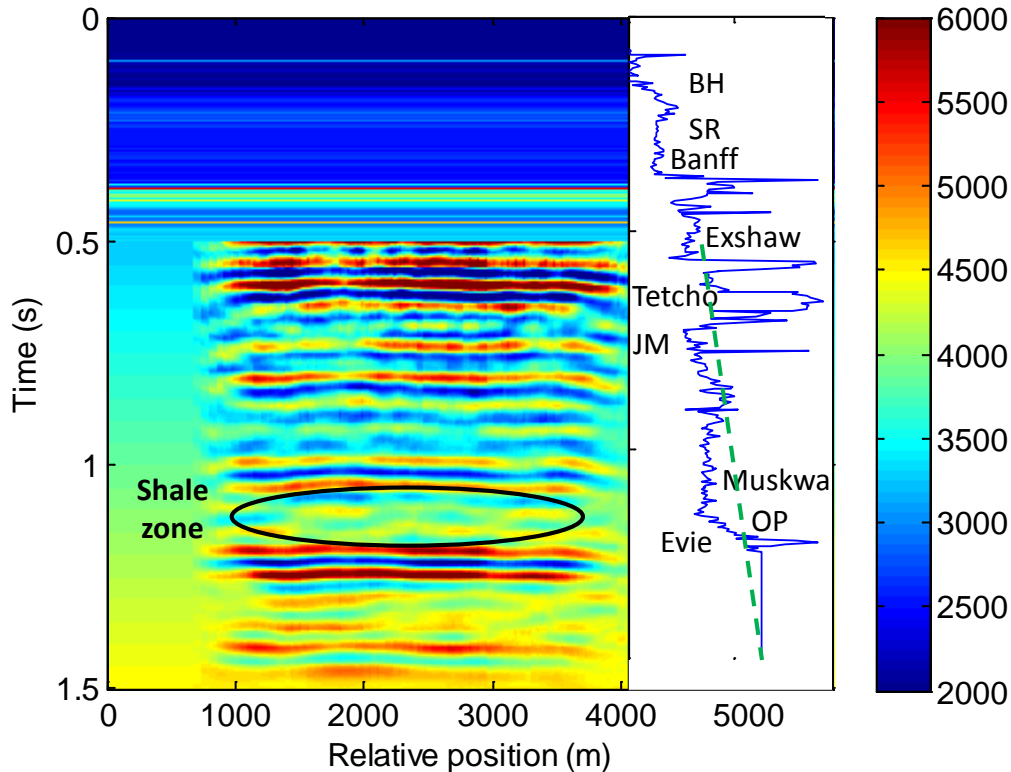


FIG. 10: Comparison of P-P inversion results correlated with overlaying sonic well log (solid blue curve). The frequency range of iterative inversion is 5 -13 HZ. Initial model is shown as green dotted line. The color scale is velocity.

Seismic data contains band limited frequencies; therefore we were restricted to do the inversion from 5Hz to 13Hz. This lack of frequency content of the source and non-linearity of the inverse problem caused ill-posedness for the result of inversion. Consequently, as shown by the color scale in Figure (10), we had to display the inversion result within the range of 2000 to 6000 m/s. However, the result of inversion shows good correlation with the well log data overlain on the figure. We also observe the variation of inverted velocities within the shale formation of the Muskwa and Otter Park (OP) as indicated inside the ellipse. These results highlight the value in employing waveform inversion for the extraction of subsurface physical properties. The simultaneous use of travel time and amplitude in the wavefield analysis provides insight to an improved understanding of shale gas reservoirs for unconventional resource development and extraction.

CONCLUSIONS

In case where the geological structure has small lateral velocity variations, the linearized solution of the seismic reflection inverse problem can be obtained using the Pre-Stack Kirchhoff Time Migration (PSTM) and corresponding forward modeling. It requires updating the velocity in time and it incorporates accurate diffraction stack weighting of the PSTM data.

We have developed an algorithm that performs waveform inversion on the mode converted P-S data. We have used the Zoeppritz solvers for amplitudes and the Double

Square Root (DSR) equation for traveltimes consideration of P-S and P-P data during the waveform inversion.

ACKNOWLEDGEMENTS

We thank the faculty, sponsors of CREWES and Nexen Inc. for their support of this work. We also would like to thank Neda Boroumand for her useful comments and suggestions.

REFERENCES

- Aki, K., and Richards, P. G., 1980, *Quantitative Seismology : Theory and Methods*, W.H. Freeman and Company. Vol. 1.
- Beylkin G., and Burridge R., 1990, Linearized inverse scattering problems in acoustics and elasticity, *Wave Motion*, **12**, 15–52,
- Bleistein, N., J. K. Cohen, and J. W. S. Jr., 2001, *Mathematics of multidimensional seismic imaging, migration, and inversion*: Springer Verlag.
- Claerbout, J. F., 1971, Toward a unified theory of reflector mapping: *Geophysics*, **36**,467-481.
- Cohen, J. K. and Bleistein, N., 1979, Velocity inversion procedure of acoustic waves: *Geophysics*, **44**, 1077-1087.
- Innanen, K., and Margrave G. F., 2011, Seismic inversion and the importance of low frequencies: CREWES annual research report, U of Calgary
- Khaniani H., Bancroft J. C., and Margrave G. F., 2012, Full waveform inversion algorithm using Common Scatter Point (CSP) gathers: *SEG Expanded Abstracts*.
- Manning, P. M., 2008, Techniques to enhance the accuracy and efficiency of finite-difference modelling for the propagation of elastic waves: PhD thesis, The University of Calgary.
- Margrave, G. F., Ferguson, R. J., and Hogan, C. M., 2011, Full Waveform Inversion (FWI) using one-way migration and well calibration: *SEG Expanded Abstracts* **30**.
- Mi Y., and Margrave G. F., 2001, Converted-wave prestack depth imaging with the nonstationary wavefield extrapolators: CREWES annual research report, U of Calgary
- Schneider, W. A., 1978, Integral formulation for migration in two and three dimensions: *Geophysics*, **43**, 49-76.
- Sears, T., S. Singh, and P. Barton, 2008, Elastic full waveform inversion of multi-component OBC seismic data: *Geophysical Prospecting*, **56**, 843–862
- Sirgue, L., and Pratt, R. G., 2004, Efficient waveform inversion and imaging: A strategy for selecting temporal frequencies: *Geophysics*, **69**, 1, 231.
- Tarantola, A., 1984a, Linearized inversion of seismic reflection data: *Geophysical Prospecting*, **32**, 998-1015.
- 1984b, Inversion of seismic reflection data in the acoustic approximation: *Geophysics*, **49**, 1259–1266.
- 1986, A strategy for nonlinear elastic inversion of seismic reflection data: *Geophysics*, **51**, 1893-1903.
- 1987, *Inverse problem theory: Methods for data fitting and model parameter estimation*: Elsevier Science Publishing Co., Inc.
- Virieux, J., and S. Operto, 2009, An overview of full-waveform inversion in exploration geophysics: *Geophysics*, **74**, WCC127-WCC152
- Yilmaz, Ö., 1989, Velocity-stack processing: *Geophysical Prospecting*, **37**, 357–382